Phase Separation Induced by Orbital Degrees of Freedom in Models for Manganites with Jahn-Teller Phonons

S. Yunoki, A. Moreo, and E. Dagotto
National High Magnetic Field Lab and Department of Physics, Florida State University, Tallahassee, Florida 32306
(Received 13 July 1998)

The 2-orbital Kondo model with classical Jahn-Teller phonons is studied using Monte Carlo techniques. The observed phase diagram is rich and includes a novel regime of phase separation induced by the orbital degrees of freedom. Experimental consequences of our results are discussed. In addition, the optical conductivity $\sigma(\omega)$ of the model is presented. It is shown to have several similarities with experimental measurements for manganites. [S0031-9007(98)08000-4]

PACS numbers: 71.10.–w, 75.10.–b, 75.30.Kz

Doped manganites are currently under much investigation due to the dramatic decrease in their resistivity when the spins order ferromagnetically by lowering the temperature T or applying a magnetic field [1]. This effect is caused by a metal-insulator transition associated with the magnetic ordering. The ferromagnetic (FM) phase is understood based on the double-exchange (DE) mechanism [2]. However, experiments on manganites have revealed a complex phase diagram that is certainly beyond the DE ideas and a more refined approach is needed to understand these compounds [3].

Since the 1950s the 1-orbital FM Kondo model for manganites has been widely studied. However, it is only recently that its computational analysis started, and surprises have already been observed [4–6]. In particular, the transition from the undoped spin-antiferromagnetic (AFM) regime to the spin-FM regime at finite hole density occurs through phase separation (PS), instead of through a canted state as believed before. A growing body of experimental results indeed indicates the existence of PS in manganites [7,8], in agreement with the theoretical calculations. PS tendencies above the FM critical temperature $T_c^{\rm FM}$ could be important to explain the colossal magnetoresistance of doped manganites.

However, in spite of its rich phase diagram the 1-orbital Kondo model is incomplete. For instance, dynamical Jahn-Teller (JT) distortions are also important [9], and a description of orbital order [10] obviously needs at least two orbitals. Such a multiorbital model with JT phonons is nontrivial [11], and the previous experience with the 1-orbital case suggests that a computational analysis beyond crude mean-field approximations is crucial to understand its properties.

It is precisely the purpose of this paper to report the first computational study of a 2-orbital model for manganites including JT phonons. The results show a rich phase diagram including a novel regime of PS induced by the orbital, rather than the spin, degrees of freedom (d.o.f.). The Hamiltonian used here has three contributions $H_{\rm KJT} = H_{\rm K} + H_{\rm JT} + H_{\rm AFM}$. The first term is

$$H_{\rm K} = -\sum_{\langle \mathbf{ij}\rangle\sigma ab} t_{ab}(c^\dagger_{\mathbf{i}a\sigma}c_{\mathbf{j}b\sigma} + \text{H.c.}) - J_{\rm H}\sum_{\mathbf{i}a\alpha\beta}\mathbf{S_i}\cdot c^\dagger_{\mathbf{i}a\alpha}\sigma_{\alpha\beta}c_{\mathbf{i}a\beta}\,, \quad (1)$$

where $\langle \mathbf{ij}\rangle$ denotes nearest-neighbor lattice sites, $J_{\rm H} > 0$ is the Hund coupling, $a, b = 1, 2$ are the two e_g orbitals, the t_{2g} spins $\mathbf{S_i}$ are assumed to be classical [12] (with $|\mathbf{S_i}| = 1$), and the rest of the notation is standard. None of the results described below depends crucially on the set $\{t_{ab}\}$ selected [13]. Throughout the paper the energy units are chosen such that $t_{11} = 1$ in the x direction. In addition, since $J_{\rm H}$ is large in the real manganites, here it will be fixed to be eight unless otherwise stated. Finally, the e_g density $\langle n\rangle$ is adjusted using a chemical potential μ.

The coupling with JT phonons is through [9]

$$H_{\rm JT} = \lambda\sum_{\mathbf{i}ab\sigma} c^\dagger_{\mathbf{i}a\sigma}Q^{ab}_{\mathbf{i}}c_{\mathbf{i}b\sigma} + \frac{1}{2}\sum_{\mathbf{i}}(Q^{(2)^2}_{\mathbf{i}} + Q^{(3)^2}_{\mathbf{i}})\,, \quad (2)$$

where $Q^{11}_{\mathbf{i}} = -Q^{22}_{\mathbf{i}} = Q^{(3)}_{\mathbf{i}}$, and $Q^{12}_{\mathbf{i}} = Q^{21}_{\mathbf{i}} = Q^{(2)}_{\mathbf{i}}$. These phonons are assumed to be classical. This approximation has been discussed in Ref. [9], where it was concluded that at temperatures of the order of the critical ones (room temperature), or a sizable fraction of them, the use of classical phonons is acceptable [14]. At very low temperatures the quantum character of phonons is important, but this is not the range of temperatures explored here. Note that $T = 1/10$ is about 200–300 K [4]. Finally, a small coupling between the t_{2g} spins is needed to account for the AFM character of, e.g., $CaMnO_3$. This Heisenberg term is $H_{\rm AFM} = J'\sum_{\langle \mathbf{ij}\rangle}\mathbf{S_i}\cdot\mathbf{S_j}$, where J' is fixed to 0.05 throughout the paper, a value compatible with experiments [15]. To study $H_{\rm KJT}$ a Monte Carlo (MC) technique was used. The trace over the e_g electrons is carried out exactly using library subroutines for a fixed background of t_{2g} spins and phonons. This background is selected based on a Metropolis MC procedure [4].

 0031-9007/98/81(25)/5612(4)$15.00

The CPU time of the technique grows rapidly with the number of sites L, but the method has the important advantage that it does not have sign problems at any T [4]. Finally, to analyze orbital correlations the pseudospin operator $\mathbf{T_i} = \frac{1}{2}\sum_{\sigma ab} c^{\dagger}_{\mathbf{i}a\sigma}\sigma_{ab}c_{\mathbf{i}b\sigma}$ is used, while for spin correlations the operator is standard. The Fourier transform of the pseudospin correlations is defined as $T(\mathbf{q}) = \frac{1}{L}\sum_{\mathbf{l},\mathbf{m}} e^{i\mathbf{q}\cdot(\mathbf{l}-\mathbf{m})}\langle \mathbf{T_m}\cdot\mathbf{T_l}\rangle$, with a similar definition for the spin structure factor $S(\mathbf{q})$.

Consider first the limit $\langle n\rangle = 1.0$ (undoped manganites). Figure 1a shows $T(q)$ and $S(q)$ at representative momenta vs λ. For small λ a large $S(0)$ indicates a tendency to spin-FM order (as in the qualitatively similar 1-orbital problem at $\langle n\rangle = 0.5$ [4]). The small values of $T(q)$ imply that in this regime the orbitals remain disordered. When the coupling reaches $\lambda_{c1} \sim 1.0$, the rapid increase of $T(\pi)$ now suggests that the ground state has a *staggered* (or "antiferro") orbital pattern, with the spins remaining FM since $S(0)$ is large [16]. The existence of this phase was discussed before using multiorbital Hubbard models [17]. Our results show that it can also be induced by JT phonons. As the coupling increases further, another transition at $\lambda_{c2} \sim 2.0$ occurs to a spin-AFM orbital-FM state [$S(\pi)$ and $T(0)$ are large]. In this region a 1-orbital approximation is suitable. Studying the spin and orbital correlations in real space leads to the same conclusions as discussed here.

The three regimes of Fig. 1a can be understood in the limit where λ and $J_{\rm H}$ are the largest scales, and using $t_{12} = t_{21} = 0$, $t_{11} = t_{22} = t$ for simplicity. For parallel spins with orbitals split in a staggered (uniform) pattern, the energy per site at lowest order in t is $\sim -t^2/\Delta$ (~ 0), where Δ is the orbital splitting. For antiparallel spins with uniform (staggered) orbital splitting, the energy is $\sim -t^2/2J_{\rm H}$ [$\sim -t^2/(2J_{\rm H}+\Delta)$]. Then, when $\Delta < 2J_{\rm H}$ ("intermediate" λ's), a spin-FM orbital-AFM order dominates, while as λ grows further a transition to a spin-AFM orbital-FM ground state is expected. This reasoning is dimension independent, as the results for a 2D cluster in Fig. 1b show. In 3D (Fig. 1c) and $J_{\rm H} = \infty$ at least two of the regimes of Fig. 1a and 1b have been identified. It was also observed that the behavior in Fig. 1a and 1b does not change when other sets $\{t_{ab}\}$ are used [13].

The next issue to be explored is the transport properties at $\langle n\rangle = 1$. The algorithm used here allows us to calculate *real-time* dynamical responses accurately, including the optical conductivity $\sigma(\omega > 0)$ [5]. From the sum rule, e_g kinetic energy, and the integral of $\sigma(\omega > 0)$, the $\omega = 0$ Drude weight D_W can be obtained. In Fig. 2a, D_W is shown for several sizes. D_W vanishes at λ_{c1} signaling a *metal-insulator* transition (MIT). Here the insulating phase is spin FM and orbital AFM, while the metallic one is spin FM and orbital disordered [18]. The density of states (DOS) for $\lambda > \lambda_{c1}$ was also calculated and it presents a clear gap at the Fermi level. Although finite-size studies for $D > 1$ are difficult, the qualitative shape of D_W vs λ on 4^2 and 4^3 clusters was found to be the same as in 1D and, thus, it is likely that the MIT exists also in $D = 2$ and 3.

Consider now the influence of hole doping on the $\langle n\rangle = 1.0$ phase diagram. The first issue to be addressed is the stability of other densities as μ is varied. Figure 2b shows $\langle n\rangle$ vs μ in the intermediate-λ regime. It is remarkable that *two* regions of unstable densities exist below some critical temperature $T_c^{\rm PS}$ (roughly $\sim 1/20$; see

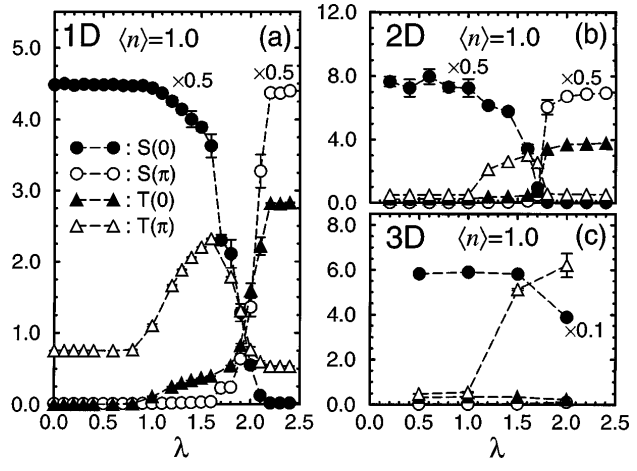

FIG. 1. (a) $T(q)$ and $S(q)$ vs λ, working at $\langle n\rangle = 1.0$, $T = 1/75$, $J_{\rm H} = 8$, $J' = 0.05$, and in 1D with ten sites. $\{t_{ab}\}$ correspond to set T_1 (see [13]); (b) same as (a) but for a 4^2 cluster, $T = 1/50$, and hopping T_3 (T_4) in the y (x) direction. $q = 0$ [π] denotes $(0,0)$ [(π,π)]; (c) same as (a) but for a 4^3 cluster, $T = 1/50$, the 3D hopping amplitudes of Ref. [13], and $J_{\rm H} = \infty$. $q = 0$ [π] denotes $(0,0,0)$ [(π,π,π)].

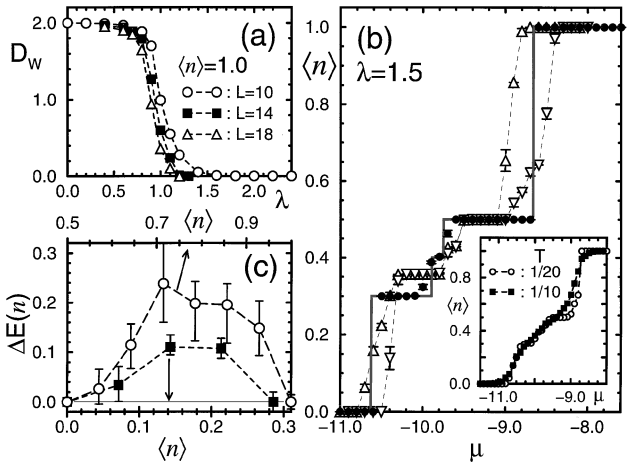

FIG. 2. (a) D_W vs λ for several chains ($T = 1/75$); (b) $\langle n\rangle$ vs μ at $\lambda = 1.5$, $L = 10$, and $T = 1/40$ (solid circles). The solid line is obtained from the Maxwell's construction. The triangles are results also at $\lambda = 1.5$ and $T = 1/40$, but using 14 sites and only 2×10^4 MC sweeps to show the appearance of *hysteresis* loops as in a first-order transition. The inset shows the T dependence of the results at $L = 10$; (c) $\Delta E(n)$ (see text) vs $\langle n\rangle$ showing a negative curvature characteristic of PS. Results at large (open circles) and small (full squares) densities are shown on a $L = 14$ cluster with periodic boundary conditions and the couplings of (b).

inset, Fig. 2b). Similar conclusions were reached using the Maxwell's construction [5]. Over 10^6 MC sweeps at each μ were needed for convergence near the unstable regions. These instabilities signal the existence of PS in the H_{KJT} model. At low density there is separation between an (i) empty e_g-electron band with AFM-ordered t_{2g} spins and a (ii) metallic spin-FM orbital-FM phase. In the unstable region near $\langle n \rangle = 1.0$ PS is between the phase (ii) mentioned above and (iii) the insulating spin FM and orbital-AFM phase described in Fig. 1a [19]. The driving force for this regime of PS is the orbital d.o.f., since the spins are uniformly ordered in both phases involved. In addition, note that these phases are also compatible with A-type AFM order (future work in 3D will address this issue). Studying $\langle n \rangle$ vs μ, for $\lambda < \lambda_{c1}$ only PS at small densities is observed, while for $\lambda > \lambda_{c2}$ the PS close to $\langle n \rangle = 1$ involves a spin-AFM orbital-FM phase [4].

To confirm that the discontinuity in $\langle n \rangle$ vs μ corresponds to phase separation, in Fig. 2c the ground state energy is provided at several densities. The results indeed have the *negative* curvature characteristic of PS, both at large and small densities. To accommodate these two important density regimes in the same plot, the energies in Fig. 2c are defined as $\Delta E(n) = E(n) - E_0(n)$, where $E(n)$ is the actual ground state energy obtained as explained in Ref. [5], and $E_0(n)$ is a straight line (zero curvature) that joins the energies of the two (stable) extremal densities of both the low- and high-density regimes. Further confirmation of the PS tendencies was obtained from the MC time evolution of n, as μ is varied.

Results in the limit $J_{\mathrm{H}} = \infty$ using a $L = 22$ site cluster are in Fig. 3a. Once again, a discontinuity in $\langle n \rangle$ vs μ was found at large and small densities, correlated with a negative curvature in the energy (not shown). Figure 3a helps in clarifying that the plateaus at densities, e.g., between 0.3 and 0.5 in Fig. 2b are caused by the intrinsic discreteness of the clusters used here. As L grows, this fine structure disappears. See, e.g., the smoothly varying density between $\langle n \rangle \sim 0.25$ and ~ 0.55 in Fig. 3a. However, the discontinuities at large and small $\langle n \rangle$ remain strong, as they should if there is PS. Similar results as found in 1D appear also in 2D systems (Fig. 3b).

Then, based on the information discussed thus far, supplemented by other MC measurements, the phase diagram of the 1D H_{KJT} model is given in Fig. 3c. The metallic spin-FM region contains two regimes: one ferro-orbital ordered and the other orbitally disordered, as deduced from the behavior of pseudospin correlations, the mean value of the pseudospin operators, and the probability of double occupancy of the same site with different orbitals. The results are similar for several $\{t_{ab}\}$ sets [13]. Our simulations suggest that the qualitative shape of Fig. 3c should be valid also in $D = 2$ and 3. In addition, at large λ the probability of double occupancy of the same site was found to be very small, mimicking the effects of a large Coulomb interaction.

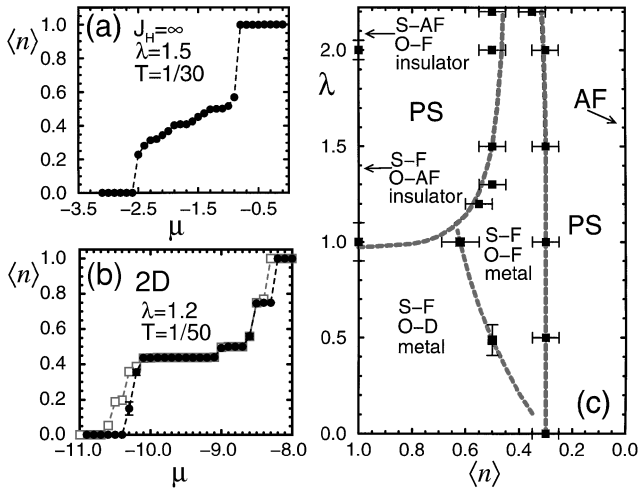

FIG. 3. (a) $\langle n \rangle$ vs μ in the limit $J_{\mathrm{H}} = \infty$, using $\lambda = 1.5$, $J' = 0.05$, $T = 1/30$, and a 22-site chain; (b) $\langle n \rangle$ vs μ at $\lambda = 1.2$ using a 4^2 cluster and at $T = 1/50$. The two sets of points that produce the hysteresis loops are obtained by increasing and decreasing μ using $\sim 10^4$ sweeps at each μ; (c) phase diagram of H_{KJT} at $J_{\mathrm{H}} = 8.0$, $J' = 0.05$, and using set T_1 for $\{t_{ab}\}$. S-F and S-AF denote regimes with FM- and AFM-spin order, respectively. O-D, O-F, and O-AF represent states with disordered, uniform, and staggered orbital order, respectively. PS means phase separation.

Consider now $\sigma(\omega)$. Experimental studies reported a broad peak at $\omega \sim 1$ eV (for hole doping $x > 0.2$ and $T > T_c^{\mathrm{FM}}$) [20,21]. At room T there is negligible weight near $\omega = 0$, but as T is reduced the 1 eV peak shifts to smaller energies, gradually transforming into a Drude response well below T_c^{FM}. The finite-ω peak can be identified even inside the FM phase. The coherent spectral weight is only a small fraction of the total.

In Fig. 4a, $\sigma(\omega)$ for the H_{KJT} model is shown at $\langle n \rangle = 0.7$ and several temperatures near the unstable PS region of Fig. 3c (weight due to J_{H} split bands is not shown, but it appears at a higher energy). Here the FM spin correlation length grows rapidly with the lattice size for $T^* \leq 0.05t$, which can be considered as the "critical" temperature. Both at high and intermediate T a broad peak is observed at $\omega \sim 1$, smoothly evolving to lower energies as T decreases. The peak can be identified below T^* as in experiments [20,21]. Eventually as the temperature is further reduced, $\sigma(\omega)$ is dominated by a Drude peak. The T dependence shown in Fig. 4a is achieved at this λ and $\langle n \rangle$ by a combination of a finite-ω phonon-induced broad feature that loses weight, and a Drude response that grows as T decreases (for smaller λ's, the two peaks can be distinguished even at the lowest temperature shown in Fig. 4a). The similarity with experiments suggests that real manganites may have couplings close to an unstable region in parameter space. In the inset, D_W vs T is shown. Note that D_W vanished suggesting a MIT. Results for the 1-orbital case are smoother.

A similar good agreement with experiments was observed working in the regime of the orbitally induced PS

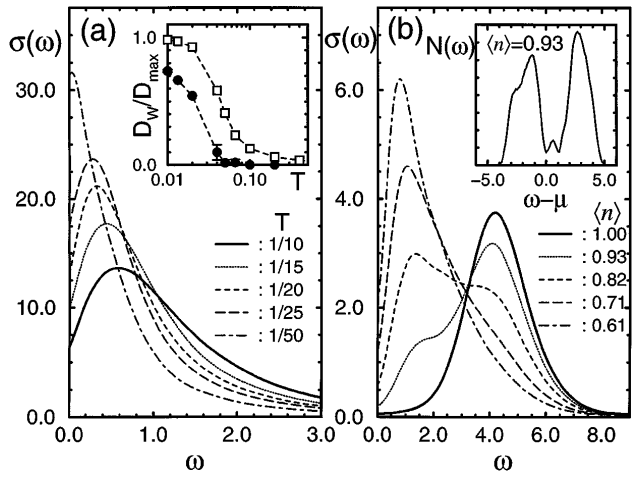

FIG. 4. (a) $\sigma(\omega)$ at $\lambda = 1.0$, $\langle n\rangle = 0.7$, and $L = 20$, and several temperatures. The inset shows D_W vs T for both the $H_{\rm KJT}$ (circles) and the 1-orbital model (squares) of Ref. [4] (the latter at $\langle n\rangle = 0.65$). D_W is normalized to the maximum value for the 1-orbital model at $T = 0.01$; (b) $\sigma(\omega)$ vs ω parametric with $\langle n\rangle$ at $\lambda = 1.5$, $T = 1/10$, and $L = 16$ (results for $L = 10$ are similar). The inset shows the lower $J_{\rm H}$-split DOS at $\langle n\rangle = 0.93$. In (a) and (b) a δ-function broadening $\epsilon = 0.25$ was used, as well as set T_1 for the hopping amplitudes.

but at a temperature above $T_c^{\rm PS}$. Here the broad feature observed at high T in Fig. 4a moves to higher energies (Fig. 4b) since λ has increased. At the temperature of Fig. 4b the system is an insulator at $\langle n\rangle = 1$, but as hole carriers are added a second peak at lower energies develops, in addition to a weak Drude peak (which carries, e.g., just 1% of the total weight at $\langle n\rangle = 0.61$). This feature at high T is reminiscent of recent experimental results [21] where a two-peak structure was observed at room T and several densities. Similar results were obtained on 4^2 clusters. In Fig. 4b the peak at large ω is caused by phononic effects since its position was found to grow rapidly with λ [$\Delta \sim 2\lambda\langle(Q_{\rm i}^{(2)^2} + Q_{\rm i}^{(3)^2})^{1/2}\rangle$]. It corresponds to intersite transitions between Mn^{3+} JT-split states. The lower energy structure is compatible with a Mn^{3+}-Mn^{4+} transition [22]. The inset of Fig. 4b shows the DOS of the system. The two peaks above μ are responsible for the features found in $\sigma(\omega)$. This interpretation is the same as given in Ref. [11] at $D = \infty$.

Summarizing, here the first computational study of the 2-orbital Kondo model including Jahn-Teller phonons was reported. The phase diagram includes regions of phase separation both at large and small e_g densities. Coulomb interactions will break the large regions involved in PS for the pure $H_{\rm KJT}$ model into small islands of one phase embedded into the other. Recalling that our spin-FM phase at $\langle n\rangle = 1$ and $D = 1, 2$ is also compatible with A-type spin-AFM order, several experimental results [7] are in agreement with the tendencies discussed in this paper. At small $\langle n\rangle$, the PS observed here could be transformed by long-range Coulomb interactions into a charge-ordered state. Note that the PS observed in electron-doped Sr_2MnO_4 [8] and other compounds [23] is also compatible with our results.

The authors are supported by the NSF Grant No. DMR-9520776.

[1] S. Jin *et al.*, Science **264**, 413 (1994).
[2] C. Zener, Phys. Rev. **82**, 403 (1951).
[3] P. E. Schiffer *et al.*, Phys. Rev. Lett. **75**, 3336 (1995).
[4] S. Yunoki *et al.*, Phys. Rev. Lett. **80**, 845 (1998); E. Dagotto *et al.*, Phys. Rev. B **58**, 6414 (1998).
[5] S. Yunoki and A. Moreo, Phys. Rev. B **58**, 6403 (1998).
[6] See also E. L. Nagaev, Phys. Status Solidi (b) **186**, 9 (1994); S-Q. Shen and Z. D. Wang, Phys. Rev. B **58**, R8877 (1998); D. P. Arovas and F. Guinea, Phys. Rev. B **58**, 9150 (1998); H. Yi and J. Yu, Phys. Rev. B **58**, 11 123 (1998); M. Yu. Kagan *et al.*, cond-mat/9804213.
[7] J. M. De Teresa *et al.*, Nature (London) **386**, 256 (1997); G. Allodi *et al.*, Phys. Rev. B **56**, 6036 (1997); M. Hennion *et al.*, Phys. Rev. Lett. **81**, 1957 (1998); J. H. Jung *et al.*, cond-mat/9809107, and references therein.
[8] Wei Bao *et al.*, Solid State Commun. **98**, 55 (1996).
[9] A. J. Millis *et al.*, Phys. Rev. Lett. **74**, 5144 (1995); H. Röder *et al.*, Phys. Rev. Lett. **76**, 1356 (1996).
[10] Y. Murakami *et al.*, Phys. Rev. Lett. **80**, 1932 (1998).
[11] Results using the $D = \infty$ approximation can be found in A. J. Millis *et al.*, Phys. Rev. B **54**, 5405 (1996).
[12] This approximation was shown to be accurate in Ref. [4].
[13] Most of the work in one dimension has been performed using $t_{11} = t_{22} = 2t_{12} = 2t_{21}$ (set T_1), but results have also been obtained with $t_{11} = t_{22}$ and $t_{12} = t_{21} = 0$ (T_2), as well as with the hopping that takes into account the proper orbital overlap, namely, $t_{11} = 3t_{22} = \sqrt{3}\,t_{12} = \sqrt{3}\,t_{21}$ (T_3) [see S. Ishihara *et al.*, Phys. Rev. B **56**, 686 (1997)]. In two dimensions the set T_1 in both directions was used, but also the combination of T_3 in the y direction and $t_{11} = 3t_{22} = -\sqrt{3}\,t_{12} = -\sqrt{3}\,t_{21}$ (T_4) in the x direction. Finally, in three dimensions T_4 was used in the x direction, T_3 in the y direction, and $t_{11} = t_{12} = t_{21} = 0$, $t_{22} = 4/3$ (T_5) in the z direction.
[14] Note that estimations of $T_c^{\rm FM}$ using quantum and classical phonons lead to very similar results [9].
[15] T. G. Perring *et al.*, Phys. Rev. Lett. **78**, 3197 (1997).
[16] $H_{\rm KJT}$ is not invariant under arbitrary pseudospin-space rotations and, thus, the Mermin-Wagner theorem does not apply to the orbital correlations.
[17] J. Goodenough, Phys. Rev. **100**, 565 (1955); K. Kugel and D. Khomskii, JETP Lett. **15**, 446 (1972); T. Mizokawa and A. Fujimori, Phys. Rev. B **56**, R493 (1997).
[18] In Ref. [11], a MIT at $\lambda \sim 1$ was also found but it was not associated with orbital order.
[19] Studies of a model with strong Coulomb interactions by S. Maekawa *et al.* also found a similar PS.
[20] M. Quijada *et al.*, cond-mat/9803201. See also S. G. Kaplan *et al.*, Phys. Rev. Lett. **77**, 2081 (1996); T. Ishikawa *et al.*, Phys. Rev. B **57**, R8079 (1998).
[21] J. H. Jung *et al.*, Phys. Rev. B **57**, R11 043 (1998); K. H. Kim *et al.*, cond-mat/9804167; cond-mat/9804284.
[22] Although its dependence with λ was weak.
[23] P. G. Radaelli *et al.* (private communication).